ACS EARTH AND SPACE CHEMISTRY

http://pubs.acs.org/journal/aesccq

Article

# Sodium Drives Interfacial Equilibria for Semi-Soluble Phosphoric and Phosphonic Acids of Model Sea Spray Aerosol Surfaces

Jennifer F. Neal,[†] Mickey M. Rogers,[†] Morgan A. Smeltzer, Kimberly A. Carter-Fenk, Alexander J. Grooms, Mia M. Zerkle, and Heather C. Allen*

Cite This: *ACS Earth Space Chem.* 2020, 4, 1549−1557

Read Online

ACCESS | Metrics & More | Article Recommendations | Supporting Information

**ABSTRACT:** Organic phosphates and phosphonates represent important yet understudied constituents in our molecular understanding of the ocean. Herein, we determined the critical concentration of sodium relating to the onset of surface activity of alkyl phosphates and phosphonates at the air−water interface to further understand the interfacial environment of sea spray aerosols emitted from the ocean's surface. A low pH range (1−5.6) was chosen to represent a model system for aged, acidic marine aerosols. The protonation state and sodium binding properties of $C_{16}$−$C_{18}$ alkyl phosphoric and phosphonic acids were explored using surface pressure−area isotherms and infrared reflection−absorption spectroscopy. We found that increasing pH and headgroup charge led to significant desorption of these semi-soluble phosphorus-containing acids into bulk solution, while the neutral, fully protonated, and sodium complexed species were favored at the interface. For the phosphonate species, the competition between sodium complexation and protonation reveals a critical sodium chloride concentration of ≥2 M at pH 2 necessary to outcompete the acid−base equilibrium. The onset of this equilibrium shift begins at concentrations as low as 0.1 M NaCl at pH 2, which demonstrates that ion pairing-mediated surface activity is highly relevant in sea spray aerosol systems. We also show that competitive interfacial equilibria between speciation and binding cannot be modeled by known bulk processes for the fully soluble methylphosphonic acid or through theoretical predictions from the Gouy−Chapman model.

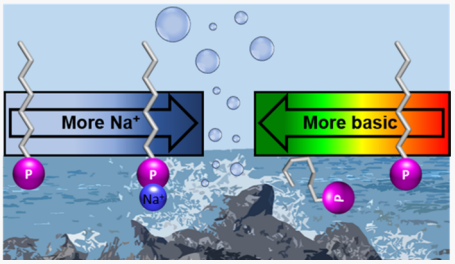


**KEYWORDS:** *air−sea interface, SSA, competition, phosphate, infrared reflection*



## INTRODUCTION

The interfacial microenvironment at the monolayer−water surface has been shown to drive strong binding enhancements,[1−5] shift acid−base speciation,[6−9] and alter the hydration environment of ions[10,11] as compared to the bulk solution equivalent. Monolayer surfaces are often utilized as a model proxy to study the thin organic coating on sea spray aerosols (SSAs), which are emitted from the ocean's surface.[12−19] SSA models thus need inputs from a molecular understanding of the unique surface properties at SSA interfaces and soluble bulk processes. We have chosen to investigate the surface properties of organic phosphorus species at low pH and high ionic strength (with NaCl) to mimic the aging process of SSAs.[20] Alkyl phosphates (C−O−P) and phosphonates (C−P) were selected to represent organic phosphorus species relevant to ocean chemistry,[21,22] wherein both moieties play key roles in marine primary production as nutrients.[23,24] Interestingly, phosphonates were found to have higher proportions in surface water than phosphates due to the lower reactivity of the organic phosphonate C−P bond.[21,25] Our study seeks to explore the molecular interactions of these species in model SSAs by studying them at the surface of aqueous solutions.

We first qualitatively determined the protonation state of these semi-soluble phosphonic and phosphoric acids (Figure 1) by following changes in surface pressure through surface concentration measurements. These semi-soluble species form insoluble monolayers as neutral species but become readily soluble in the solution upon deprotonation. Interfacial acid−base equilibria (apparent surface p$K_a$s) are still widely debated in the literature and often vary from the p$K_a$s of the bulk solution equivalents.[6−9,26−33] Previous studies of amphiphilic phosphoric and phosphonic acids revealed significant changes in intermolecular interactions and hydration as a result of varying pH.[33−36] Thus, we utilized surface pressure−area isotherms to study changes in the monolayer phases to gain insight into the noncovalent interactions between molecules. We predicted that these intermolecular interactions will be greatly affected by speciation changes for the tightly packed single-chain species. Infrared reflection−absorption spectros-

**Received:** May 14, 2020
**Revised:** July 7, 2020
**Accepted:** July 14, 2020
**Published:** July 14, 2020

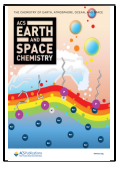

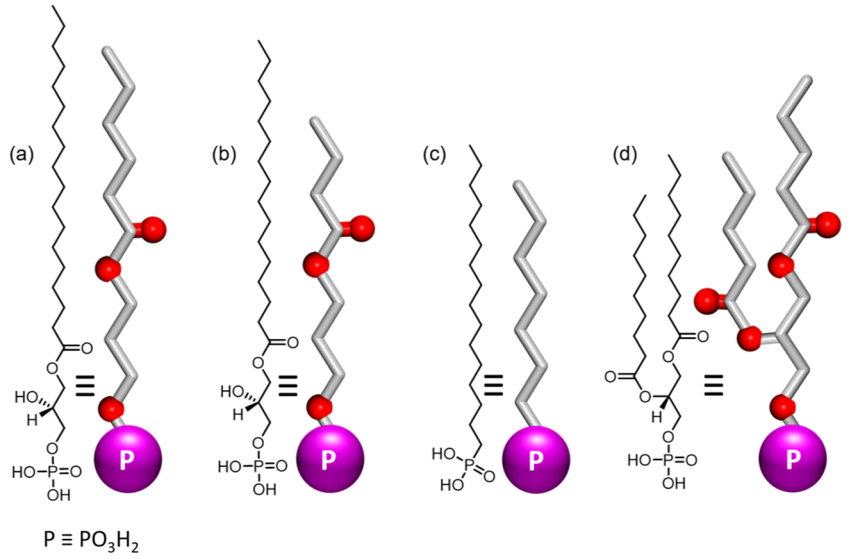


**Figure 1.** Structures of the compounds used in this study shown in their fully protonated forms. (a) 1-stearoyl lysophosphatidic acid ($C_{18}$ LPA), (b) 1-palmitoyl lysophosphatidic acid ($C_{16}$ LPA), (c) hexadecylphosphonic acid ($C_{16}$ phosphonic), and (d) 1,2-didecanoyl-3-phosphatidic acid (didecanoyl PA). Hydroxyl groups are omitted in the schematic representations of $C_{16}$ and $C_{18}$ LPA for simplicity.

copy (IRRAS) was also used to probe the vibrational modes of the molecules as pH and surface concentration change. IRRAS is a surface-sensitive spectroscopic technique that probes the molecular monolayer by measuring reflectance-absorbance (RA) of the monolayer surface, RA = $-\log(R_m/R_o)$, where $R_m$ is the reflectivity of the monolayer and $R_o$ is the reflectivity of the solution absent of the monolayer.[37] Ultimately, we observed the onset of the speciation changes from neutral to singly deprotonated for these semi-soluble phosphonic and phosphoric acids in the low pH range studied between pH 1 and 5.6. Our results demonstrate that the change in surface speciation has a profound impact on the surface concentration and the resulting surface coating of SSAs.

Additionally, we seek to unravel the complexity of interfacial equilibria. The single-chain phosphonic acid species was chosen for this model study because phosphonic acids are highly relevant but underexplored in the atmospheric community, although results can be applied to the phosphate moiety as well. Figure 2 shows the phosphonic acid equilibria expressions for the acid–base equilibrium and the sodium complexation at low pH. By controlling the pH and sodium chloride concentration, we drove the acid–base equilibrium of the phosphonic acid and phosphonate and the sodium complexation equilibrium of phosphonate binding to sodium cations. At a constant pH of 2 (chosen to mimic an acidic aerosol[38]), the competitive effects of these processes were studied by shifting the competitive equilibria through a constant addition of NaCl. In doing so, we have resolved the concentration of sodium (≥2 M at pH 2) necessary to outcompete the acid–base protonation equilibrium. Results from this study illustrate that sodium can drive speciation changes at the aqueous surface. Effectively, low pH and sodium binding are competitive processes in which modulating the pH and sodium concentration can shift the speciation of the phosphonic acid species. We chose to interrogate the changing state of the phosphonic acid for this model system plus our results are applicable to other marine relevant, acidic species including phospholipids and fatty acids, among others.

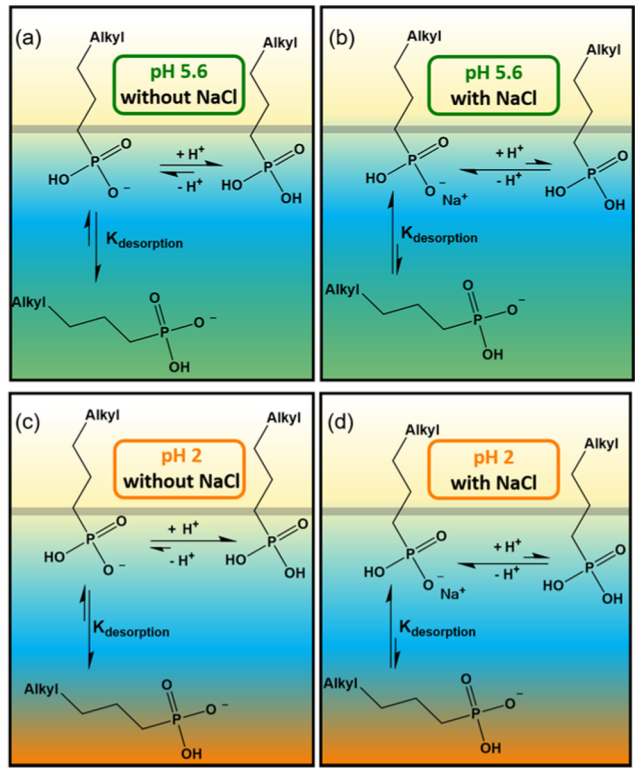


**Figure 2.** Competitive equilibria at the air–water interface. (a) Schematic representation of the acid–base equilibrium resulting in the desorption of the deprotonated phosphonate species at pH 5.6, (b) sodium complexation to the phosphonate headgroup and driven to the interface at pH 5.6, (c) acid–base equilibrium of phosphonate and phosphonic acid at pH 2, and (d) competitive equilibria between acid–base and sodium complexation at pH 2 with high sodium chloride concentrations.

The unique properties at aqueous interfaces were previously shown to drive different speciation and binding equilibria compared to the bulk solution equivalent.[3,4,6] The low dielectric constant at the aqueous interface, which decreases


https://dx.doi.org/10.1021/acsearthspacechem.0c00132
ACS Earth Space Chem. 2020, 4, 1549–1557

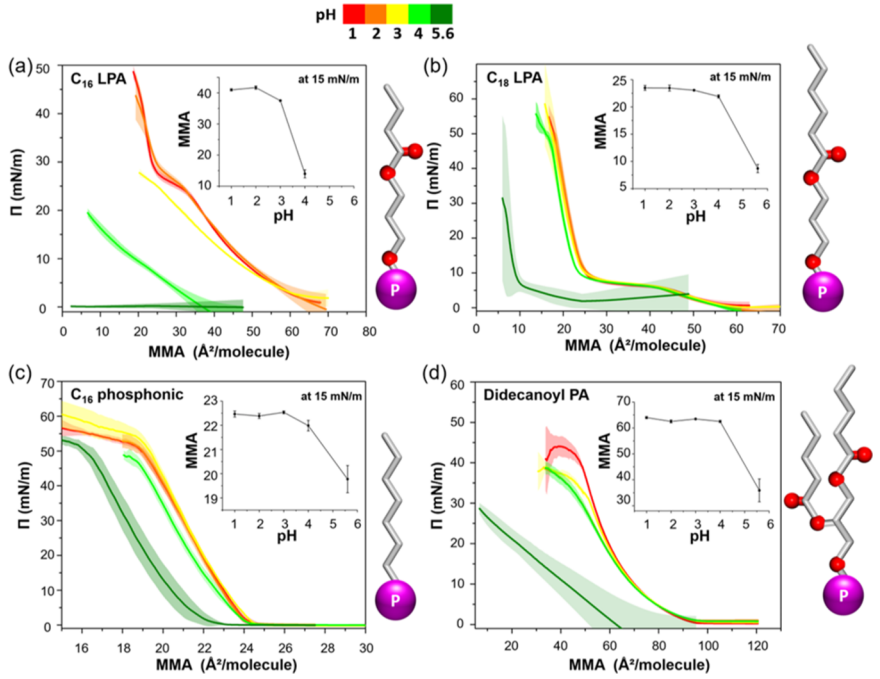


**Figure 3.** Surface pressure (Π)−area (A) compression isotherms and apparent mean molecular areas (MMAs) taken at Π = 15 mN/m for (a) $C_{16}$ LPA, (b) $C_{18}$ LPA, (c) $C_{16}$ phosphonic acid, and (d) didecanoyl PA on pH 1, 2, 3, 4, and water. Shaded bands represent one standard deviation. Desorption of the monolayer is revealed as a shift to lower apparent MMAs as pH is increased.

to ∼2 in the topmost layers,[39] has a profound impact on the acid−base speciation, which should inherently shift with the changing dielectric environment.[40] Furthermore, the preorganization of surface-active species confines the molecules to a discrete microenvironment, which influences the protonation state and sodium complexation through changes in noncovalent interactions and packing arrangements.[41] Results from our study reveal that the competition between protonation and sodium binding can be controlled and predicted at a critical sodium chloride concentration ≥2 M at pH 2. Our model system of semi-soluble phosphate and phosphonate species shows that the interfacial microenvironment is key for a molecular understanding of the stability, speciation, and binding in SSA interfaces and opens up exciting new avenues for future research on SSAs.

## RESULTS AND DISCUSSION

The goal of this work is to determine both the critical role of pH and sodium binding for a series of semi-soluble phosphate and phosphonate species at the aqueous surface. Infrared reflection−absorption spectroscopy (IRRAS) and surface pressure (Π)−mean molecular area (A) compression isotherms were performed with several short-chain species: (a) $C_{18}$ lysophosphatidic acid ($C_{18}$ LPA), (b) $C_{16}$ lysophosphatidic acid ($C_{16}$ LPA), (c) $C_{16}$ phosphonic acid, and (d) didecanoyl phosphatidic acid (didecanoyl PA) to study surface activity (Figure 3). This set of molecules differs in several features including alkyl and acyl chain length, headgroup, and number of chains. Overall, we aim to tune these molecular features to determine their impacts on surface activity, protonation state, and sodium complexation.

We first explore properties of the phosphate and phosphonate semi-soluble species without sodium chloride to establish that they are in fact fully protonated at pH 2. Π−A isotherms for $C_{16}$ and $C_{18}$ LPA, $C_{16}$ phosphonic acid, and didecanoyl PA are shown in the pH range 1−5.6 (Figure 3). The acidic pH range (1−5.6) was initially chosen to avoid the addition of bases such as sodium hydroxide and circumvent potential issues related to sodium binding to the negative monolayer and countercation charge screening.[42]

Π−A isotherms for these semi-soluble species are shifted to lower apparent mean molecular areas (MMAs) as pH increases in the aqueous subphase. We define the apparent MMA as a lowering of the experimentally observed MMA due to the depletion of molecules in the monolayer. The shift in the apparent MMA is attributed to the desorption of the deprotonated, semi-soluble charged species into bulk solution as the pH increases (Figure 3). These results indicate that the fully protonated, neutral species are more favorable at the aqueous interface, in agreement with previous studies.[43,44] The apparent MMAs at a constant Π = 15 mN/m are plotted for each trial to compare results across different pH values (Figure 3, insets). The plot for $C_{16}$ LPA shows a sharp drop in MMA between pH 3 and pH 4, indicating that the charged species becomes more dominant and the semi-soluble species begins to desorb into bulk solution in this pH range. Desorption of $C_{18}$ LPA occurs between pH 4 and pH 5.6, which is higher than the pH range observed for the $C_{16}$ LPA desorption. Although the chain lengths differ by only two methylene units, there is a remarkable change in the isotherms at the same pH for these molecules. There are greater dispersion forces upon lengthening the chain length, which acts to increase the surface propensity of the $C_{18}$ LPA. As the packing density and molecular environment changes, so should the acid−base dissociation properties. Another plausible explanation in the literature contributes this result to strong intermolecular interactions between headgroups because it is more difficult to deprotonate phosphate in a hydrogen-bonding network with neighboring phosphates.[6,32,45]


https://dx.doi.org/10.1021/acsearthspacechem.0c00132
ACS Earth Space Chem. 2020, 4, 1549−1557

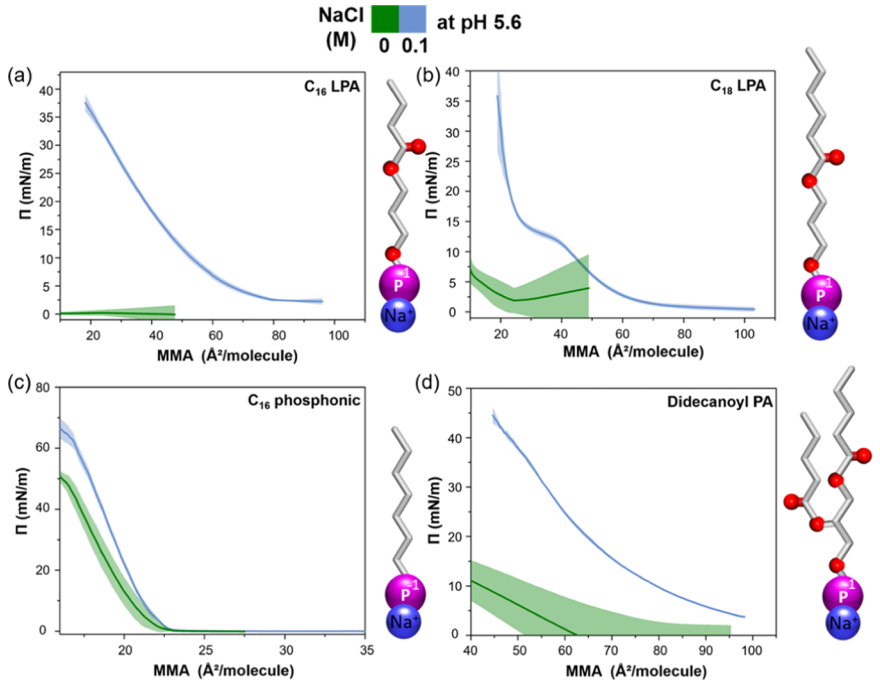


**Figure 4.** Surface pressure (Π)−area (A) compression isotherms for (a) $C_{16}$ LPA, (b) $C_{18}$ LPA, (c) $C_{16}$ phosphonic acid, and (d) didecanoyl PA on 0.1 M NaCl at pH 5.6 and pH 5.6 without NaCl. The shaded region represents one standard deviation above and below the mean.

The $C_{16}$ phosphonic acid and the didecanoyl PA showed a similar shift in apparent MMA with increasing pH (Figure 3c,d). In addition to the $C_{16}$ phosphonic acid and didecanoyl PA, we also studied the $C_{18}$ phosphonic acid and dioctanoyl PA, but these did not form a semi-soluble species (Supporting Information (SI), Figure S1a,b). The $C_{18}$ phosphonic acid did not desorb but instead formed an insoluble monolayer on both water (pH 5.6) and low pH, whereas the dioctanoyl PA remained semi-soluble at pH 1.[46−49] The Π−A isotherms agree with results from IRRAS, which are shown in the Supporting Information (SI, Figure S2). IRRAS spectra of these molecules at pH 1 and pH 5.6 show a net loss of the semi-soluble species with increasing pH. The speciation of these semi-soluble species is controlled by acid−base equilibria in the pH range 1−5.6 without the addition of sodium chloride. Consistently, Brewster angle microscopy (BAM) is an imaging technique used to visualize morphological changes in a surface from its reflection of light without contribution from the solution. BAM images of these semi-soluble species reveal changes in packing structure in the low pH range (SI, Figures S3−S5).[50] Whereas the isotherms at pH 5.6 showed some extent of desorption for all of the semi-soluble species, the addition of 0.1 M sodium chloride restores the surface activity of the molecular monolayer (Figure 4), consistent with prior work of palmitic acid and sodium chloride.[42] Sodium binds to the phosphonate through electrostatically driven interactions, which was previously shown to be an influential driving force in the low dielectric constant regime of the air−water interface.[3] With the knowledge that sodium chloride addition plays an influential role in surface activity, we sought to study the competition between sodium complexation and protonation.

We used the $C_{16}$ phosphonic acid for our model system to study the effects of sodium chloride addition at low pH. The IRRAS spectra of the $C_{16}$ phosphonic acid at pH 2 (Figure 5a) and pH 5.6 (Figure 5b) shows significant changes with increasing sodium chloride concentrations. All vibrational assignments for the $C_{16}$ phosphonic acid surfactant were approximated using density functional theory at the B3LYP/6-31G* level of theory (SI, Figure S6, Tables S1 and S2).[51−55] We assign the peak at ∼942 $cm^{-1}$ to the symmetric phosphonate $\nu_s$ (O = P−$O^-$) stretch, which appears with increasing sodium concentrations. This peak is diagnostic to determine the protonation state because it is not present in the phosphonic acid spectrum at pH 2 until 2 M (Figure 5b). Furthermore, the bending mode $\delta$(POH)[56] at ∼998 $cm^{-1}$ undergoes a red shift upon sodium addition (Figure 5c). As the negatively charged $C_{16}$ phosphonate electrostatically interacts with sodium present in the solution, the environment of the phosphonate headgroup changes and we observe this as a shift in the $\delta$(POH) mode. This is indicative of metal binding or electron transfer from the bound sodium to the phosphonate headgroup as previously shown.[57,58] The shift is sometimes also correlated with a change in intensity and is consistent with a change in headgroup orientation and transition moment strength. Even at a pH of 2, sodium begins to drive phosphonic acid toward the phosphonate−sodium complex.

We normalized the peak positions of the $\delta$(POH) mode with sodium addition to our lowest and highest values (where "0" corresponds to the peak position at pH 2 without NaCl and "1" corresponds to the peak at pH 5.6 with 1 M NaCl) (Figure 6a). Our results demonstrate that the precipice of the phosphonate−sodium binding begins at concentrations >0.1 M NaCl and saturates at concentrations ≥2 M NaCl at pH 2.

We demonstrate that the speciation of the $C_{16}$ phosphonic species is highly influenced by the presence of sodium. We propose that the protonation state of the $C_{16}$ phosphonic species can be controlled and shifted even at low pH based on our experimental evidence. To compare our experimental results with established theory, we employed the Gouy−Chapman model modified with the Grahame equation, as detailed in Tyrode and Corkery, 2018.[59] While there are


https://dx.doi.org/10.1021/acsearthspacechem.0c00132
ACS Earth Space Chem. 2020, 4, 1549−1557

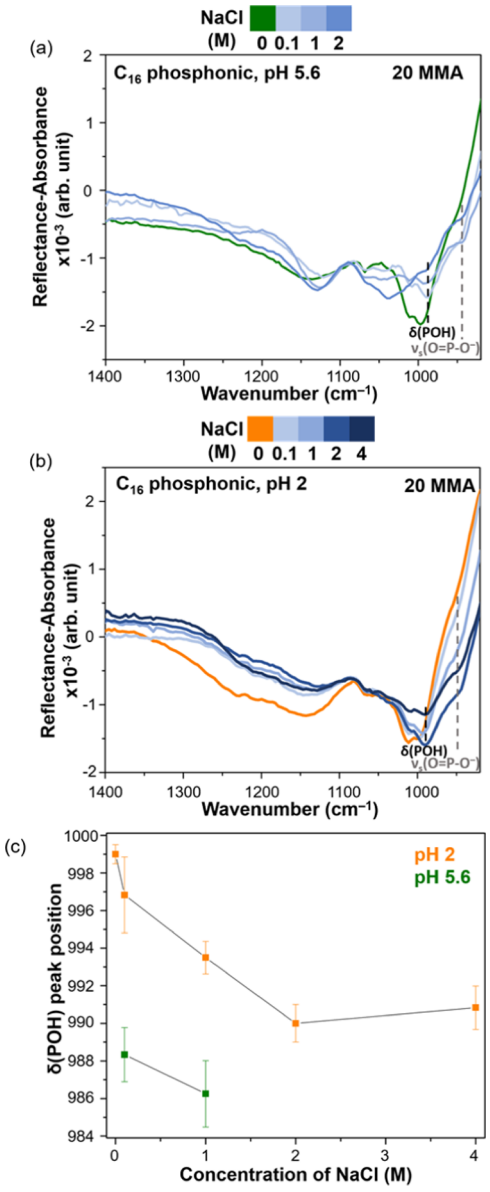


**Figure 5.** (a) $C_{16}$ phosphonate species binding to increasing concentrations of sodium at pH 5.6, (b) at a constant pH of 2, sodium addition begins to shift the speciation of phosphonic acid to the phosphonate species due to electrostatically driven binding, (c) average peak position is plotted to show the stark changes resulting from sodium binding shifting the speciation at a constant pH of 2.

several models to consider, and despite its simple assumptions, the Gouy−Chapman model describes the electrostatic double layer quite well for aqueous solutions containing monovalent salts.[60] More detail about the Gouy−Chapman calculation and surface model is discussed in the Supporting Information, Section 3. This model is used to calculate the theoretical degree of deprotonation ($\alpha$) with increasing sodium chloride concentrations, $[NaCl]_\infty$ (eq 1).[59,61]

$$\frac{A_M}{\alpha e}\sinh\left[\frac{1}{2}\left(\ln[H^+]_\infty - \ln K_a - \ln\left(\frac{1-\alpha}{\alpha}\right)\right)\right] = (8\varepsilon\varepsilon_0 kT[NaCl]_\infty)^{-1/2} \quad (1)$$

Where $A_M$ is the mean molecular area (20 Å$^2$ per phosphonate molecule), $e$ is the elementary charge, $K_a$ is the acid dissociation constant ($pK_a$ = 2.13), $\varepsilon$ is the dielectric constant of water, $\varepsilon_0$ is the permittivity of free space, and $k$ is the Boltzmann constant.

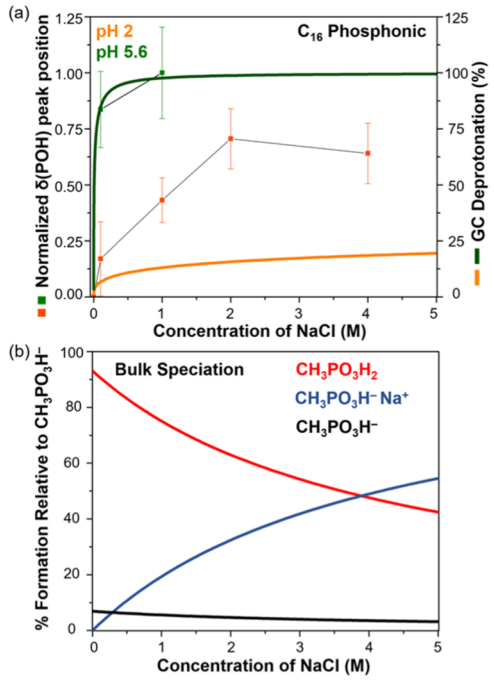


**Figure 6.** (a) Normalized peak position of the $\delta$(POH) mode at pH 2 with increasing sodium addition on the left axis and the predicted speciation of the $C_{16}$ phosphonic acid based on the Gouy−Chapman (GC) model ($pK_a$ = 2.13, pH 2 and pH 6) on the right axis. At pH 5.6 (upper curve), the $C_{16}$ phosphonate species follows the Gouy−Chapman (GC) model; however, at pH 2, there is a large disagreement between the experiment and the model. This demonstrates the incompatibility of the GC model for predicting sodium binding interactions of the $C_{16}$ phosphonate species at low pH. (b) Bulk equilibria of methylphosphonic acid predicted using HySS software.

The degree of deprotonation was solved for a bulk $[H^+]$ concentration corresponding to pH = 2 and 6. Figure 6a shows the results of this prediction alongside the normalized $\delta$(POH) peak positions. Results of phosphonic acid at pH 5.6 are consistent with Gouy−Chapman if we consider the $C_{16}$ phosphonic acid at pH 5.6 with 1 M NaCl to be fully deprotonated and bound to sodium. The model fails to recognize the influence of high sodium addition at low pH and dramatically underestimates the degree of deprotonation at pH 2. Our results demonstrate clearly that Gouy−Chapman breaks down at high concentrations, consistent with other reports.[62−65]

We also compared our experimental result to the bulk solution equivalent to confirm that the interfacial environment cannot be modeled by known bulk processes. The water-soluble species methylphosphonic acid was chosen for the bulk model. Methylphosphonic acid has a weak binding constant to sodium ($K_{complex} = 10^{0.54}$)[66] and a $pK_{a1}$ of 2.13.[67] By inputting these values in hyperquad simulation and speciation software (HySS),[68] we can predict the critical sodium concentration necessary to outcompete the protonation equilibrium in bulk solution. Figure 6b shows the predicted speciation with HySS in which it takes concentrations exceeding 4 M sodium chloride to begin to outcompete the acid−base equilibria at a pH of 1. Clearly, bulk values cannot be used to explain our


https://dx.doi.org/10.1021/acsearthspacechem.0c00132
ACS Earth Space Chem. 2020, 4, 1549−1557

observations at the air−water interface, confirming that the interfacial microenvironment can drive complex speciation.

Under the typical basic pH conditions of the ocean (pH ∼ 8.1−8.2) and ignoring the contributions of salts, the semi-soluble species will be deprotonated and desorb into bulk solution, as depicted in Figure 7a. However, in an acidic aged

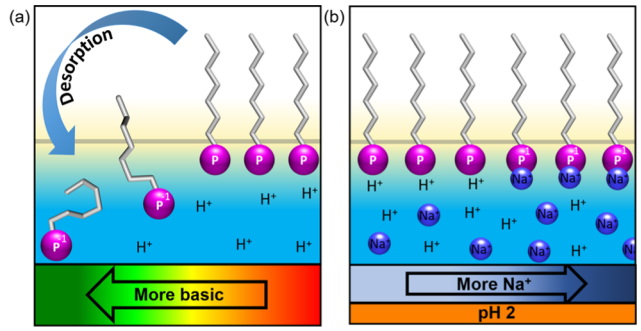


**Figure 7.** Schematic representation of the (a) desorption of the $C_{16}$ phosphonate species into bulk solution and (b) the competition between speciation and sodium complexation.

aerosol environment, where conditions possibly transcend a pH of 2, the species will be fully protonated and become surface active (Figure 7a). However, there is also a competition between protonation and sodium binding that must be considered (Figure 7b). At a critical sodium chloride concentration of 2 M in an acidic pH 2 environment, the interfacial acid−base equilibrium will shift, which results in enhanced sodium binding to the phosphonate species.

## SURFACE ATMOSPHERIC IMPLICATIONS

Our study demonstrates the importance of competitive binding and its relationship to the partitioning of semi-soluble species to the interfacial regime for aged SSAs. As SSAs acidify in the atmosphere, aerosol chemistry will change as the semi-soluble species restructure the air−water interface.[69] Moreover, in aged, acidic environments, there will be a competition between ion complexation and protonation state. This is particularly relevant for molecules with an acidic headgroup. Additionally, phosphonates represent an important yet understudied component of marine phosphorus. The phosphonate species 2-aminoethyl-phosphonic acid comprises 10% of the dissolved organic phosphorus in the ocean,[22] and in general, phosphonates are found in lipids and macromolecular material of several marine phyla.[70] 2-aminoethyl-phosphonic acid is the primary phosphorus source and product of several oceanic bacteria,[24] prokaryotic phytoplankton, and other aquatic organisms.[22,70] Due in part to their abundance and C−P stability, which renders them more resistant to hydrolysis, the long-chain phosphonates should demonstrate strong surface activity.[71−74]

Our study helps further the molecular understanding of semi-soluble phosphonates and phosphates and their surface activity. As wave-breaking processes in the ocean form foams and entrained bubble plumes, these biological surfactants, dependent on chain length and under the right conditions as shown here, will partition to the air−water interface, resulting in the formation and release of SSA with an organic coating.[75−77] It is reasonable to expect semi-soluble species to undergo increased sodium interaction via aerosol aging or evaporation during an airborne lifetime.[20,78] Additionally, as the protonated phosphonic acids and sodium-bound phosphonates reside at aerosol surfaces, they will participate differently in heterogeneous chemistry with atmospheric gases, further changing the SSA composition.[79,80] There will be changes in packing density, mixing properties, and intermolecular interactions in the different pH environments as speciation changes, which will also greatly affect gas uptake. Finally, the competition studies between protonation speciation and sodium complexation demonstrate that even at low pH, the semi-soluble species binds to sodium and effectively outcompetes the protonation equilibria. This opens questions about the irrelevance of $pK_a$ and the relevance of ion pairing, as metal ions are shown here to outcompete protonation even at low pH. Moreover, aerosols that travel from marine regions to more arid continental regions will be impacted by evaporative effects.[81−86] Once the sodium concentration reaches 2 M (at ∼ a 75% loss of water[87]), the partitioning of semi-soluble species from $Na^+$ complexation will then be stabilized in the interfacial region and will not desorb into the bulk aqueous phase. This scenario shows a turnover point of ≥2 M NaCl concentration and provides a lower limit given that more strongly interacting metal ions (e.g., $Mg^{2+}$, $Ca^{2+}$, and transition metal ions) will also be available for complexation. This situation gives rise to increasing surface stability of semi-soluble species at the aqueous interface.

## CONCLUSIONS

The competition between binding and acid−base speciation is an important concept for sea spray aerosol modeling that warrants further exploration. Our results illustrate that surface activity is highly influenced by pH (1−5.6) and low concentrations of sodium chloride for a series of semi-soluble phosphoric and phosphonic acids. We studied the phosphonic acid species further in a competition study between speciation and sodium complexation at low pH to model an acidic, aged sea spray aerosol. Our results reveal that there is a critical concentration of sodium chloride (≥2 M) at pH 2 to begin shifting the interfacial equilibria toward the deprotonated phosphonate species. We demonstrate that in an acidified aerosol environment, the concentration of sodium cations can be more influential than pH to determine the protonation state of organic acidic species.

## ASSOCIATED CONTENT

### Supporting Information

The Supporting Information is available free of charge at https://pubs.acs.org/doi/10.1021/acsearthspacechem.0c00132.

Experimental details, Π-A isotherms of the $C_{18}$ phosphonic acid and dioctanoyl PA surfactants, IRRAS spectra of $C_{16}$ LPA, $C_{18}$ LPA, and the $C_{16}$ phosphonic acid on pH 1 and pH 5.6 at 20 MMA, and didecanoyl PA on pH 1 and pH 5.6 at 50 MMA, vibrational assignments for the phosphonic acid species using density functional theory (DFT) at the B3LYP/6-31G* level of theory, Gouy−Chapman deprotonation calculation and discussion, and BAM images of $C_{16}$ LPA at 30 MMA, $C_{18}$ LPA at 21 MMA, the $C_{16}$ phosphonic acid at 20 MMA, didecanoyl PA at 60 MMA at pH 1, 2, 3, 4, and 5.6 (PDF)


https://dx.doi.org/10.1021/acsearthspacechem.0c00132
ACS Earth Space Chem. 2020, 4, 1549−1557

## AUTHOR INFORMATION


### Corresponding Author

**Heather C. Allen** − *Department of Chemistry & Biochemistry, The Ohio State University, Columbus, Ohio 43210, United States;* orcid.org/0000-0003-3120-6784; Phone: +1-614-292-4707; Email: allen@chemistry.ohio-state.edu; Fax: +1-614-292-1685

### Authors

**Jennifer F. Neal** − *Department of Chemistry & Biochemistry, The Ohio State University, Columbus, Ohio 43210, United States*

**Mickey M. Rogers** − *Department of Chemistry & Biochemistry, The Ohio State University, Columbus, Ohio 43210, United States*

**Morgan A. Smeltzer** − *Department of Chemistry & Biochemistry, The Ohio State University, Columbus, Ohio 43210, United States*

**Kimberly A. Carter-Fenk** − *Department of Chemistry & Biochemistry, The Ohio State University, Columbus, Ohio 43210, United States*

**Alexander J. Grooms** − *Department of Chemistry & Biochemistry, The Ohio State University, Columbus, Ohio 43210, United States*

**Mia M. Zerkle** − *Department of Chemistry & Biochemistry, The Ohio State University, Columbus, Ohio 43210, United States*

Complete contact information is available at: https://pubs.acs.org/10.1021/acsearthspacechem.0c00132

### Author Contributions

†J.F.N and M.M.R. contributed equally to this work


### Notes

The authors declare no competing financial interest.

## ACKNOWLEDGMENTS

Funding for this research was provided by the National Science Foundation (NSF), the MSN program in the CHE division, under grant CHE-1609672. We acknowledge partial support by NSF through the Center for Aerosol Impacts on Chemistry of the Environment (CAICE), CHE-1801971 (M.M.R. and K.A.C.-F.). Data archiving is underway at the UC San Diego Library Digital Collections for CAICE website: https://library.ucsd.edu/dc/collection/bb96275693. The authors declare no competing financial interest. The authors would like to thank Kevin Carter-Fenk, Taylor A. Neal, and Ting Zhang for valuable discussions.

## REFERENCES


(1) Sasaki, D. Y.; Kurihara, K.; Kunitake, T. Self-Assembled Multifunctional Receptors for Nucleotides at the Air-Water Interface. *J. Am. Chem. Soc.* **1992**, *114*, 10994−10995.

(2) Onda, M.; Yoshihara, K.; Koyano, H.; Ariga, K.; Kunitake, T. Molecular Recognition of Nucleotides by the Guanidinium Unit at the Surface of Aqueous Micelles and Bilayers. A Comparison of Microscopic and Macroscopic Interfaces. *J. Am. Chem. Soc.* **1996**, *118*, 8524−8530.

(3) Neal, J. F.; Zhao, W.; Grooms, A. J.; Smeltzer, M. A.; Shook, B. M.; Flood, A. H.; Allen, H. C. Interfacial Supramolecular Structures of Amphiphilic Receptors Drive Aqueous Phosphate Recognition. *J. Am. Chem. Soc.* **2019**, *141*, 7876−7886.

(4) Neal, J. F.; Zhao, W.; Grooms, A. J.; Flood, A. H.; Allen, H. C. Arginine−Phosphate Recognition Enhanced in Phospholipid Monolayers at Aqueous Interfaces. *J. Phys. Chem. C* **2018**, *122*, 26362−26371.

(5) Burrows, S. M.; Gobrogge, E.; Fu, L.; Link, K.; Elliott, S. M.; Wang, H.; Walker, R. OCEANFILMS-2: Representing Coadsorption of Saccharides in Marine Films and Potential Impacts on Modeled Marine Aerosol Chemistry. *Geophys. Res. Lett.* **2016**, *43*, 8306−8313.

(6) Wellen, B. A.; Lach, E. A.; Allen, H. C. Surface PKa of Octanoic, Nonanoic, and Decanoic Fatty Acids at the Air-Water Interface: Applications to Atmospheric Aerosol Chemistry. *Phys. Chem. Chem. Phys.* **2017**, *19*, 26551−26558.

(7) Griffith, E. C.; Vaida, V. Ionization State of L-Phenylalanine at the Air−Water Interface. *J. Am. Chem. Soc.* **2013**, *135*, 710−716.

(8) Coddens, E. M.; Angle, K. J.; Grassian, V. H. Titration of Aerosol pH through Droplet Coalescence. *J. Phys. Chem. Lett.* **2019**, *10*, 4476−4483.

(9) Schiffer, J. M.; Luo, M.; Dommer, A. C.; Thoron, G.; Pendergraft, M.; Santander, M. V.; Lucero, D.; Pecora de Barros, E.; Prather, K. A.; Grassian, V. H.; et al. Impacts of Lipase Enzyme on the Surface Properties of Marine Aerosols. *J. Phys. Chem. Lett.* **2018**, *9*, 3839−3849.

(10) Flores, S. C.; Kherb, J.; Cremer, P. S. Direct and Reverse Hofmeister Effects on Interfacial Water Structure. *J. Phys. Chem. C* **2012**, *116*, 14408−14413.

(11) Allen, H. C.; Casillas-Ituarte, N. N.; Sierra-Hernández, M. R.; Chen, X.; Tang, C. Y. Shedding Light on Water Structure at Air−Aqueous Interfaces: Ions, Lipids, and Hydration. *Phys. Chem. Chem. Phys.* **2009**, *11*, 5538−5549.

(12) Carter-Fenk, K. A.; Allen, H. C. Collapse Mechanisms of Nascent and Aged Sea Spray Aerosol Proxy Films. *Atmosphere* **2018**, *9*, 503.

(13) Elliott, S.; Burrows, S.; Cameron-Smith, P.; Hoffman, F.; Hunke, E.; Jeffery, N.; Liu, Y.; Maltrud, M.; Menzo, Z.; Ogunro, O.; et al. Does Marine Surface Tension Have Global Biogeography? Addition for the OCEANFILMS Package. *Atmosphere* **2018**, *9*, 216.

(14) Elliott, S.; Burrows, S. M.; Deal, C.; Liu, X.; Long, M.; Ogunro, O.; Russell, L. M.; Wingenter, O. Prospects for Simulating Macromolecular Surfactant Chemistry at the Ocean−Atmosphere Boundary. *Environ. Res. Lett.* **2014**, *9*, No. 064012.

(15) Burrows, S. M.; Ogunro, O.; Frossard, A. A.; Russell, L. M.; Rasch, P. J.; Elliott, S. M. A Physically Based Framework for Modeling the Organic Fractionation of Sea Spray Aerosol from Bubble Film Langmuir Equilibria. *Atmos. Chem. Phys.* **2014**, *14*, 13601−13629.

(16) Elliott, S.; Menzo, Z.; Jayasinghe, A.; Allen, H. C.; Ogunro, O.; Gibson, G.; Hoffman, F.; Wingenter, O. Biogeochemical Equation of State for the Sea-Air Interface. *Atmosphere* **2019**, *10*, 230.

(17) Schiffer, J. M.; Mael, L. E.; Prather, K. A.; Amaro, R. E.; Grassian, V. H. Sea Spray Aerosol: Where Marine Biology Meets Atmospheric Chemistry. *ACS Cent. Sci.* **2018**, *4*, 1617−1623.

(18) Bertram, T. H.; Cochran, R. E.; Grassian, V. H.; Stone, E. A. Sea Spray Aerosol Chemical Composition: Elemental and Molecular Mimics for Laboratory Studies of Heterogeneous and Multiphase Reactions. *Chem. Soc. Rev.* **2018**, *47*, 2374−2400.

(19) Cochran, R. E.; Ryder, O. S.; Grassian, V. H.; Prather, K. A. Sea Spray Aerosol: The Chemical Link between the Oceans, Atmosphere, and Climate. *Acc. Chem. Res.* **2017**, *50*, 599−604.

(20) Fridlind, A. M.; Jacobson, M. Z. A Study of Gas-Aerosol Equilibrium and Aerosol pH in the Remote Marine Boundary Layer during the First Aerosol Characterization Experiment (ACE 1). *J. Geophys. Res.: Atmos.* **2000**, *105*, 17325−17340.

(21) Kolowith, L. C.; Ingall, E. D.; Ronald, B. Composition and Cycling of Marine Organic Phosphorus. *Limnol. Oceanogr.* **2001**, *46*, 309−320.

(22) Whitney, L. P.; Lomas, M. W. Phosphonate Utilization by Eukaryotic Phytoplankton. *Limnol. Oceanogr. Lett.* **2019**, *4*, 18−24.

(23) Karl, D. M. Microbially Mediated Transformations of Phosphorus in the Sea: New Views of an Old Cycle. *Annu. Rev. Mater. Res.* **2014**, *6*, 279−337.

(24) Dyhrman, S. T.; Benitez-Nelson, C. R.; Orchard, E. D.; Haley, S. T.; Pellechia, P. J. A Microbial Source of Phosphonates in Oligotrophic Marine Systems. *Nat. Geosci.* **2009**, *2*, 696−699.

(25) Clark, L. L.; Ingall, E. D.; Benner, R. Marine Phosphorus Is Selectively Remineralized. *Nature* **1998**, *393*, 426.
(26) Ariga, K.; Lee, M. V.; Labuta, J.; Okamoto, K.; Hill, J. P. Studies on Langmuir Monolayers of Polyprenyl Phosphates towards a Possible Scenario for Origin of Life. *Colloids Surf., B* **2009**, *74*, 426−435.
(27) Zhang, T.; Brantley, S. L.; Verreault, D.; Dhankani, R.; Corcelli, S. A.; Allen, H. C. Effect of pH and Salt on Surface-pKa of Phosphatidic Acid Monolayers. *Langmuir* **2018**, *34*, 530−539.
(28) Kanicky, J. R.; Shah, D. O. Effect of Degree, Type, and Position of Unsaturation on the pKa of Long-Chain Fatty Acids. *J. Colloid Interface Sci.* **2002**, *256*, 201−207.
(29) Eugene, A. J.; Pillar, E. A.; Colussi, A. J.; Guzman, M. I. Enhanced Acidity of Acetic and Pyruvic Acids on the Surface of Water. *Langmuir* **2018**, *34*, 9307−9313.
(30) Mishra, H.; Enami, S.; Nielsen, R. J.; Stewart, L. A.; Hoffmann, M. R.; Goddard, W. A.; Colussi, A. J. Brønsted Basicity of the Air−Water Interface. *Proc. Natl. Acad. Sci. U.S.A.* **2012**, *109*, 18679−18683.
(31) Cheng, J.; Psillakis, E.; Hoffmann, M. R.; Colussi, A. J. Acid Dissociation versus Molecular Association of Perfluoroalkyl Oxoacids: Environmental Implications. *J. Phys. Chem. A* **2009**, *113*, 8152−8156.
(32) Kanicky, J. R.; Poniatowski, A. F.; Mehta, N. R.; Shah, D. O. Cooperativity among Molecules at Interfaces in Relation to Various Technological Processes: Effect of Chain Length on the pKa of Fatty Acid Salt Solutions. *Langmuir* **2000**, *16*, 172−177.
(33) Parreira, H. C. The Surface Chemistry of Alkyl Phosphoric Acids. *J. Colloid Sci.* **1965**, *20*, 742−754.
(34) Gershfeld, N. L.; Pak, C. Y. O. The Surface Chemistry of Monooctadecyl Phosphate at the Air/Water Interface. A Study of Molecular Aggregation in Monolayers. *J. Colloid Interface Sci.* **1967**, *23*, 215−220.
(35) Schulz, E. P.; Piñeiro, Á.; Miñones, J.; Miñones Trillo, J.; Frechero, M. A.; Pieroni, O.; Schulz, P. C. Effect of Ionization on the Behavior of *n*-Eicosanephosphonic Acid Monolayers at the Air/Water Interface. Experimental Determinations and Molecular Dynamics Simulations. *Langmuir* **2015**, *31*, 2269−2280.
(36) Zhang, T.; Cathcart, M. G.; Vidalis, A. S.; Allen, H. C. Cation Effects on Phosphatidic Acid Monolayers at Various pH Conditions. *Chem. Phys. Lipids* **2016**, *200*, 24−31.
(37) Grooms, A. J.; Neal, J. F.; Ng, K. C.; Zhao, W.; Flood, A. H.; Allen, H. C. Thermodynamic Signatures of the Origin of Anti-Hofmeister Selectivity for Phosphate at Aqueous Interfaces. *J. Phys. Chem. A* **2020**, *124*, 5621−5630.
(38) Keene, W. C.; Savoie, D. L. The pH of Deliquesced Sea-Salt Aerosol in Polluted Marine Air. *Geophys. Res. Lett.* **1998**, *25*, 2181−2184.
(39) Fumagalli, L.; Esfandiar, A.; Fabregas, R.; Hu, S.; Ares, P.; Janardanan, A.; Yang, Q.; Radha, B.; Taniguchi, T.; Watanabe, K.; et al. Anomalously Low Dielectric Constant of Confined Water. *Science* **2018**, *360*, 1339−1342.
(40) Juffer, A. H.; Vogel, H. J. pKa Calculations of Calbindin $D_{9k}$: Effects of $Ca^{2+}$ Binding, Protein Dielectric Constant, and Ionic Strength. *Proteins: Struct., Funct., Bioinf.* **2000**, *41*, 554−567.
(41) Cram, D. J. The Design of Molecular Hosts, Guests, and Their Complexes (Nobel Lecture). *Angew. Chem., Int. Ed.* **1988**, *27*, 1009−1020.
(42) Adams, E. M.; Wellen, B. A.; Thiraux, R.; Reddy, S. K.; Vidalis, A. S.; Paesani, F.; Allen, H. C. Sodium-Carboxylate Contact Ion Pair Formation Induces Stabilization of Palmitic Acid Monolayers at High pH. *Phys. Chem. Chem. Phys.* **2017**, *19*, 10481−10490.
(43) Eisenthal, K. B. Liquid Interfaces Probed by Second-Harmonic and Sum-Frequency Spectroscopy. *Chem. Rev.* **1996**, *96*, 1343−1360.
(44) Bhattacharyya, K.; Sitzmann, E. V.; Eisenthal, K. B. Study of Chemical Reactions by Surface Second Harmonic Generation: *p*-Nitrophenol at the Air−Water Interface. *J. Chem. Phys.* **1987**, *87*, 1442−1443.
(45) McLean, D. S.; Vercoe, D.; Stack, K. R.; Richardson, D. The Colloidal pKa, of Lipophilic Extractives Commonly Found in Pinus Radiata. *Appita J.* **2005**, *58*, 362−366.
(46) Ries, H. E.; Cook, H. D. Monomolecular Films of Mixtures: I. Stearic Acid with Isostearic Acid and with Tri-*p*-cresyl Phosphate. Comparison of Components with Octadecylphosphonic Acid and with Tri-*o*-xenyl Phosphate. *J. Colloid Sci.* **1954**, *9*, 535−546.
(47) Woodward, J. T.; Ulman, A.; Schwartz, D. K. Self-Assembled Monolayer Growth of Octadecylphosphonic Acid on Mica. *Langmuir* **1996**, *12*, 3626−3629.
(48) He, W.; Jiang, C.; Liu, F.; Tai, Z.; Liang, Y.; Guo, Z.; Zhu, L. Monolayer Formation of Alkyl Chain-Containing Phosphoric Acid Amphiphiles at the Air/Water (pH 5.6) Interface: Influence of Temperature and Cations. *J. Colloid Interface Sci.* **2002**, *246*, 335−342.
(49) Spink, J. A. Ionization of Monolayers of Fatty Acids from $C_{14}$ to $C_{18}$. *J. Colloid Sci.* **1963**, *18*, 512−525.
(50) Adams, E. M.; Allen, H. C. Palmitic Acid on Salt Subphases and in Mixed Monolayers of Cerebrosides: Application to Atmospheric Aerosol Chemistry. *Atmosphere* **2013**, *4*, 315−336.
(51) Shao, Y.; Gan, Z.; Epifanovsky, E.; Gilbert, A. T. B.; Wormit, M.; Kussmann, J.; Lange, A. W.; Behn, A.; Deng, J.; Feng, X.; et al. Advances in Molecular Quantum Chemistry Contained in the Q-Chem 4 Program Package. *Mol. Phys.* **2015**, *113*, 184−215.
(52) Becke, A. D. Density-Functional Thermochemistry. III. The Role of Exact Exchange. *J. Chem. Phys.* **1993**, *98*, 5648−5652.
(53) Barone, V.; Cossi, M. Quantum Calculation of Molecular Energies and Energy Gradients in Solution by a Conductor Solvent Model. *J. Phys. Chem. A* **1998**, *102*, 1995−2001.
(54) Takano, Y.; Houk, K. N. Benchmarking the Conductor-like Polarizable Continuum Model (CPCM) for Aqueous Solvation Free Energies of Neutral and Ionic Organic Molecules. *J. Chem. Theory Comput.* **2005**, *1*, 70−77.
(55) Scott, A. P.; Radom, L. Harmonic Vibrational Frequencies: An Evaluation of Hartree−Fock, Møller−Plesset, Quadratic Configuration Interaction, Density Functional Theory, and Semiempirical Scale Factors. *J. Phys. Chem. A.* **1996**, *100*, 16502−16513.
(56) Podstawka-Proniewicz, E.; Andrzejak, M.; Kafarski, P.; Kim, Y.; Proniewicz, L. M. Vibrational Characterization of L-Valine Phosphonate Dipeptides: FT-IR, FT-RS, and SERS Spectroscopy Studies and DFT Calculations. *J. Raman Spectrosc.* **2011**, *42*, 958−979.
(57) Morel, A.-L.; Boujday, S.; Méthivier, C.; Krafft, J.-M.; Pradier, C.-M. Biosensors Elaborated on Gold Nanoparticles, a PM-IRRAS Characterisation of the IgG Binding Efficiency. *Talanta* **2011**, *85*, 35−42.
(58) Munro, C. H.; Smith, W. E.; Garner, M.; Clarkson, J.; White, P. C. Characterization of the Surface of a Citrate-Reduced Colloid Optimized for Use as a Substrate for Surface-Enhanced Resonance Raman Scattering. *Langmuir* **1995**, *11*, 3712−3720.
(59) Tyrode, E.; Corkery, R. Charging of Carboxylic Acid Monolayers with Monovalent Ions at Low Ionic Strengths: Molecular Insight Revealed by Vibrational Sum Frequency Spectroscopy. *J. Phys. Chem. C* **2018**, *122*, 28775−28786.
(60) Peng, M.; Nguyen, A. V. Adsorption of Ionic Surfactants at the Air-Water Interface: The Gap between Theory and Experiment. *Adv. Colloid Interface Sci.* **2020**, *275*, No. 102052.
(61) Sthoer, A.; Hladílková, J.; Lund, M.; Tyrode, E. Molecular Insight into Carboxylic Acid−Alkali Metal Cations Interactions: Reversed Affinities and Ion-Pair Formation Revealed by Non-Linear Optics and Simulations. *Phys. Chem. Chem. Phys.* **2019**, *21*, 11329−11344.
(62) Shapovalov, V. L.; Brezesinski, G. Breakdown of the Gouy−Chapman Model for Highly Charged Langmuir Monolayers: Counterion Size Effect. *J. Phys. Chem. B* **2006**, *110*, 10032−10040.
(63) Torrie, G. M.; Valleau, J. P. Electrical Double Layers. 4. Limitations of the Gouy−Chapman Theory. *J. Phys. Chem. B.* **1982**, *86*, 3251−3257.


https://dx.doi.org/10.1021/acsearthspacechem.0c00132
*ACS Earth Space Chem.* 2020, 4, 1549−1557

(64) Loosley-Millman, M. E.; Rand, R. P.; Parsegian, V. A. Effects of Monovalent Ion Binding and Screening on Measured Electrostatic Forces between Charged Phospholipid Bilayers. *Biophys. J.* **1982**, *40*, 221−232.
(65) Kilic, M. S.; Bazant, M. Z.; Ajdari, A. Steric Effects in the Dynamics of Electrolytes at Large Applied Voltages. I. Double-Layer Charging. *Phys. Rev. E* **2007**, *75*, 21502.
(66) Alderighi, L.; Vacca, A.; Cecconi, F.; Midollini, S.; Chinea, E.; Dominguez, S.; Valle, A.; Dakternieks, D.; Duthie, A. Interaction of Beryllium(II) in Aqueous Solution with Bidentate Ligands Containing Phosphonate Groups. *Inorg. Chim. Acta* **1999**, *285*, 39−48.
(67) Popov, K.; Rönkkömäki, H.; Lajunen, L. H. J. Critical Evaluation of Stability Constants of Phosphonic Acids (IUPAC Technical Report). *Pure Appl. Chem.* **2001**, *73*, 1641−1677.
(68) Alderighi, L.; Gans, P.; Ienco, A.; Peters, D.; Sabatini, A.; Vacca, A. Hyperquad Simulation and Speciation (HySS): A Utility Program for the Investigation of Equilibria Involving Soluble and Partially Soluble Species. *Coord. Chem. Rev.* **1999**, *184*, 311−318.
(69) Menzo, Z. M.; Elliott, S.; Hartin, C. A.; Hoffman, F. M.; Wang, S. Climate Change Impacts on Natural Sulfur Production: Ocean Acidification and Community Shifts. *Atmosphere* **2018**, *9*, 167.
(70) Hilderbrand, R. L. *The Role of Phosphonates in Living Systems*; CRC Press, Inc., 1983.
(71) Rott, E.; Steinmetz, H.; Metzger, J. W. Organophosphonates: A Review on Environmental Relevance, Biodegradability and Removal in Wastewater Treatment Plants. *Sci. Total Environ.* **2018**, *615*, 1176−1191.
(72) Huang, J.; Su, Z.; Xu, Y. The Evolution of Microbial Phosphonate Degradative Pathways. *J. Mol. Evol.* **2005**, *61*, 682−690.
(73) Nowack, B. Environmental Chemistry of Phosphonates. *Water Res.* **2003**, *37*, 2533−2546.
(74) Nowack, B.; Stone, A. T. The Influence of Metal Ions on the Adsorption of Phosphonates onto Goethite. *Environ. Sci. Technol.* **1999**, *33*, 3627−3633.
(75) Meskhidze, N.; Petters, M. D.; Tsigaridis, K.; Bates, T.; O'Dowd, C.; Reid, J.; Lewis, E. R.; Gantt, B.; Anguelova, M. D.; Bhave, P. V.; et al. Production Mechanisms, Number Concentration, Size Distribution, Chemical Composition, and Optical Properties of Sea Spray Aerosols. *Atmos. Sci. Lett.* **2013**, *14*, 207−213.
(76) Stokes, M. D.; Deane, G. B.; Prather, K.; Bertram, T. H.; Ruppel, M. J.; Ryder, O. S.; Brady, J. M.; Zhao, D. A Marine Aerosol Reference Tank System as a Breaking Wave Analogue for the Production of Foam and Sea-Spray Aerosols. *Atmos. Meas. Tech.* **2013**, *6*, 1085−1094.
(77) Cochran, R. E.; Laskina, O.; Jayarathne, T.; Laskin, A.; Laskin, J.; Lin, P.; Sultana, C.; Lee, C.; Moore, K. A.; Cappa, C. D.; et al. Analysis of Organic Anionic Surfactants in Fine and Coarse Fractions of Freshly Emitted Sea Spray Aerosol. *Environ. Sci. Technol.* **2016**, *50*, 2477−2486.
(78) Jimenez, J. L.; Canagaratna, M. R.; Donahue, N. M.; Prevot, A. S. H.; Zhang, Q.; Kroll, J. H.; DeCarlo, P. F.; Allan, J. D.; Coe, H.; Ng, N. L.; et al. Evolution of Organic Aerosols in the Atmosphere. *Science* **2009**, *326*, 1525−1529.
(79) Shaloski, M. A.; Gord, J. R.; Staudt, S.; Quinn, S. L.; Bertram, T. H.; Nathanson, G. M. Reactions of $N_2O_5$ with Salty and Surfactant-Coated Glycerol: Interfacial Conversion of $Br^-$ to $Br_2$ Mediated by Alkylammonium Cations. *J. Phys. Chem. A* **2017**, *121*, 3708−3719.
(80) Atkinson, R.; Winer, A. M.; Pitts, J. N. Estimation of Night-Time $N_2O_5$ Concentrations from Ambient $NO_2$ and $NO_3$ Radical Concentrations and the Role of $N_2O_5$ in Night-Time Chemistry. *Atmos. Environ.* **1986**, *20*, 331−339.
(81) Metcalf, A. R.; Boyer, H. C.; Dutcher, C. S. Interfacial Tensions of Aged Organic Aerosol Particle Mimics Using a Biphasic Microfluidic Platform. *Environ. Sci. Technol.* **2016**, *50*, 1251−1259.
(82) O'Brien, R. E.; Wang, B.; Kelly, S. T.; Lundt, N.; You, Y.; Bertram, A. K.; Leone, S. R.; Laskin, A.; Gilles, M. K. Liquid−Liquid Phase Separation in Aerosol Particles: Imaging at the Nanometer Scale. *Environ. Sci. Technol.* **2015**, *49*, 4995−5002.
(83) Rovelli, G.; Miles, R. E. H.; Reid, J. P.; Clegg, S. L. Accurate Measurements of Aerosol Hygroscopic Growth over a Wide Range in Relative Humidity. *J. Phys. Chem. A* **2016**, *120*, 4376−4388.
(84) Nandy, L.; Liu, S.; Gunsbury, C.; Wang, X.; Pendergraft, M. A.; Prather, K. A.; Dutcher, C. S. Multistep Phase Transitions in Sea Surface Microlayer Droplets and Aerosol Mimics Using Microfluidic Wells. *ACS Earth Space Chem.* **2019**, *3*, 1260−1267.
(85) Freedman, M. A. Phase Separation in Organic Aerosol. *Chem. Soc. Rev.* **2017**, *46*, 7694−7705.
(86) Losey, D. J.; Parker, R. G.; Freedman, M. A. pH Dependence of Liquid-Liquid Phase Separation in Organic Aerosol. *J. Phys. Chem. Lett.* **2016**, *7*, 3861−3865.
(87) Millero, F. J. *Chemical Oceanography*, 4th ed.; CRC Press: Boca Raton, FL, 2013.


https://dx.doi.org/10.1021/acsearthspacechem.0c00132
*ACS Earth Space Chem.* 2020, 4, 1549−1557